Int. J. Heat Mass Transfer. Vol. 28, No. 4, pp. 837–850, 1985
Printed in Great Britain

0017-9310/85 $3.00 + 0.00
Pergamon Press Ltd.

Large eddy structure and heat transfer of turbulent natural convection along a vertical flat plate

K. KITAMURA, M. KOIKE, I. FUKUOKA and T. SAITO

Department of Energy Engineering, Toyohashi University of Technology, Tempaku-cho, Toyohashi 440, Japan

(*Received* 2 *July* 1984)

Abstract—Turbulent transport in a natural convection was investigated experimentally. Main concerns were paid to the large eddy motions existing in a turbulent boundary layer along a vertical flat plate. Visualizations of temperature and velocity fields in the wall region were mainly conducted, and it was revealed that the large eddy motions play an important role on the turbulent transport. The length and time scales of these eddies were defined and measured. Also, the coherent structure of the eddies was discussed.

1. INTRODUCTION

THE PROBLEMS of turbulent natural convection along a vertical flat plate are of considerable interest in many application fields of heat transfer. Numerous experimental studies have, therefore, been carried out to make clear the fundamental mechanisms of turbulent heat and momentum transfer. Most of the early experimental works have been limited to the measurements of the overall and local heat transfer coefficients, or of the mean temperature distributions within the turbulent boundary layer. This has been mainly due to the difficulties in measuring the velocities of extremely low magnitude in the unsteadily fluctuating temperature field.

With the recent developments in various measuring techniques and equipments such as the Laser Doppler Velocimeter or the computer-assisted Constant Temperature Anemometer, the quantitative data of turbulent velocity and temperature fluctuations have become available by the works of Cheesewright [1], Vliet and Liu [2], Smith [3], Hoogendroorn and Euser [4], Hishida *et al.* [5], Miyamoto *et al.* [6], and a few others. These data are helpful to investigate the characteristics of buoyant driven flow, but show the serious scatters in the correlations between velocity and temperature fluctuations, and especially in the Reynolds shear stress distributions.

On the other hand, in the turbulent boundary layer of forced convection, the organized or ordered motions of large scale eddies, which were observed by the visualization study of Kline *et al.* [7] in detail, have attracted much attention of many workers, and have been confirmed to play an important role on the turbulent transport of heat and momentum. In the turbulent boundary layer of natural convection, however, it has been uncertain whether the ordered motions of large scale eddies exist or not.

Considering the above, the structures of the turbulent boundary layer are investigated experimentally in the present study with the special emphasis on the large eddy motions. For the simplicity of experimental conditions, the two-dimensional boundary layers developing along vertical flat plates, which are heated with uniform heat flux, are treated. The experiments are performed both with air and water in a wide range of modified Rayleigh numbers up to the highest $Ra^* \simeq 6 \times 10^{16}$.

It is revealed that the large scale eddies comparable to those of bursting phenomena in a forced convection exist in the turbulent boundary layer of natural convection. In order to obtain the quantitative information about these eddies, the length and time scales of the large eddies are measured both from the visualized data and from the short time correlations of the temperature fluctuations. The coherent or ordered structures of the large eddy motions are also discussed by introducing the characteristic time and length scales of a natural convection.

The present results, which are focused on the large eddy motions, will be applicable to the interpretation of quantitative data obtained by the previous workers, and also give a definite image of the turbulent transport in a natural convection boundary layer.

2. EXPERIMENTAL APPARATUS AND MEASUREMENT

2.1. *Experimental apparatus*

For the generalization of the experimental results, especially those with the time and length scales of streaky patterns described in section 3, the experiments with different sizes of heat transfer surfaces and thermal properties of fluids should be performed. Therefore, the test plates of three different dimensions in height and width, given in Table 1, were designed and fabricated. Air and water were used as the working fluids. Each heat transfer plate consists of 10-mm thick plywood plates and stainless-steel foil heaters, 30 μm thick. The heaters were glued on both surfaces of the plywood plates and were connected in series and then heated by an AC power supply to attain a uniform heat flux throughout the test surface. The surface temperatures of the heated plates were measured by chromel–alumel thermocouples of 70 μm in diameter, which were spot-welded behind the heater at a constant interval in the flow direction.

NOMENCLATURE

f	frequency of streak
$\hat{f}$	non-dimensional frequency of streak, f/f_T
f_T	characteristic time scale, $(\nu/\lambda_L^2)_w$
g	gravitational acceleration
Gr_x	Grashof number, $g\beta(T_w-T_\infty)X^3/\nu^2$
Gr_x^*	modified Grashof number, $g\beta q_w X^4/\kappa\nu^2$
h	heat transfer coefficient, $q_w/(T_w-T_\infty)$
Nux	local heat transfer coefficient, hX/κ
Pr	Prandtl number, ν/α
q	heat flux
Ra	Rayleigh number, $Gr_x \cdot Pr$
Ra^*	modified Rayleigh number, $Gr_x^* \cdot Pr$
R_z	cross-correlation coefficient of temperature fluctuations at spanwise distance Z, $\overline{t_0' t_z'}/\sqrt{\overline{t_0'^2}}\sqrt{\overline{t_z'^2}}$
R_τ	auto-correlation coefficient of temperature fluctuations at time delay τ, $\overline{t_0' t_\tau'}/\sqrt{\overline{t_0'^2}}\sqrt{\overline{t_\tau'^2}}$
T	time-averaged temperature
t'	temperature fluctuation
u'	longitudinal velocity fluctuation
u^*	friction velocity, $\sqrt{\tau_w/\rho}$
v'	normal velocity fluctuation
X	height from the bottom of test plate
Y	distance from the wall
Y^+	non-dimensional distance from the wall, Yu^*/ν
Z	spanwise distance
X, Y, Z	Cartesian coordinates.

Greek symbols

α	thermal diffusivity of fluid
β	coefficient of volume expansion
ζ	non-dimensional distance from the wall, $Nu_x \cdot Y/X$
κ	thermal conductivity of fluid
λ	spanwise distance between streaks
λ_L	characteristic length scale, $(\kappa\nu^2/g\beta q)_w^{1/4}$
$\hat{\lambda}$	non-dimensional spacing between streaks, λ/λ_L
ν	kinematic viscosity
ρ	density of fluid
τ	delay time.

Superscript

$\bar{}$	time-averaged.

Subscripts

f	reference temperature
w	at wall
x	at location X
λ	based on spanwise distance
∞	at environment.

The side plates were also installed at the right and left sides of the heated plates in order to prevent the incoming flow, which would disrupt the two-dimensionality of the boundary layer. The bottom of the heated plate was 20 cm from the floor and sharp-edged to lessen the disturbances introduced towards a leading edge. The schematical illustration of the test plate is shown in Fig. 1.

The apparatus of No. I was installed vertically in a room of 130 m^3, in volume, enclosed with vinyl sheets. The apparatus of No. II and No. III were settled in the rectangular vessels of cross-sectional areas 1×1 m^2, 2×1 m^2, and heights 2.7 and 6.8 m, respectively. The large dimensions of apparatus No. III enabled the experiments with the high Rayleigh number up to $Ra^* \simeq 6 \times 10^{16}$, which was considered as the maximum limit in the laboratory framework.

2.2. *Visualization techniques*

The surface temperature distributions of the test plate were visualized by using a liquid crystal in the case of water. This liquid crystal reflects definite colors at specific range of temperatures, e.g. 30–35°C. The color ranges from clear at environmental temperature, through red as the temperature increases, and then to yellow, green, and finally, blue. These color changes are reversible. Further information about the treatments of liquid crystal can be referred to Kasagi [8]. In this experiment, the liquid crystal was purchased as a sheet, which consisted of the liquid crystal

Table 1. Heat transfer plates of present experiment

Apparatus No.	Height H (mm)	Width W (mm)	Width of heaters $W1$ (mm)	Number of heaters	Fluid	Heat flux (W m^{-2})	Maximum Ra^*
I	3,650	915	150	4	Air	40–150	5×10^{13}
II	2,500	770	150	4	Water	1,500–6,500	5×10^{15}
III	7,000	915	300	2	Air	25–75	5×10^{14}
	6,500	915	300	2	Water	1,500–4,500	6×10^{16}

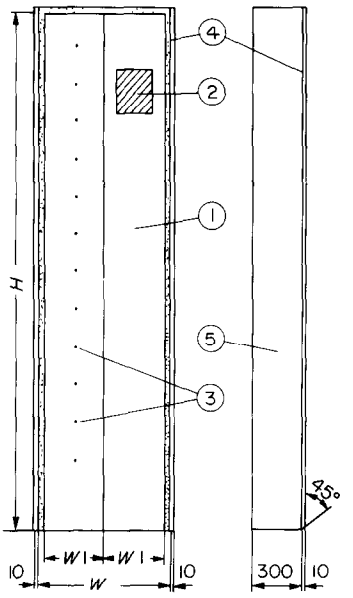

FIG. 1. Heat transfer plate.

sandwiched between a black-painted and a transparent polyethylene sheet 50 μm thick and 150×200 mm^2 in area. The response time of a color change was estimated less than 1 s, and it was sufficient to visualize the streaky patterns of the surface temperatures mentioned in the next section.

The flow visualizations were also made by using a hydrogen-bubble method for water and a smoke-wire method for air. The ascending velocities of bubbles and smoke were measured in the stagnant water and air, and were confirmed to be much smaller than those induced by a natural convection, in the range of our experiments. The fluid motions can, therefore, be traced by the bubbles and smoke.

2.3. *Measurements of temperature fluctuations and their correlations*

Each of the auto and cross correlation coefficients of temperature fluctuations in a turbulent boundary layer was measured to obtain the time and length scales of the large eddies, respectively. Quartz-coated single wire hot-film probes (Thermos-Science Inc., Type 1210-60W) and tungsten wire probes 5 μm in diameter were used as the resistance thermometers for water and air, respectively.

Their output signals were stored by a digital data recorder and then, calculated by a personal computer through a GP-IB interface. Before performing the data acquisition, the sampling frequencies and the numbers of sampling data were varied systematically to obtain reproducible results, and it turned out that the sampling frequencies of 10 Hz for water and 20 Hz for air are most appropriate in view of the traceability of the eddy motions. The numbers of sampling data were decided as 4096 in most cases for both air and water to save the CPU time and memory size. Although this number was somewhat smaller in comparison with that for the forced convection, the computed result showed no appreciable deviations from those obtained with much larger data volume.

3. RESULTS AND DISCUSSIONS

3.1. *Local heat transfer coefficients*

The local heat transfer coefficients along the flow direction were obtained for each heat transfer plate in order to classify the laminar, transition, and turbulent flow regimes. Representative data for both water and air in the case of apparatus No. III are shown in Fig. 2, where the local Nusselt numbers are plotted with modified Rayleigh numbers.

The surface heat flux was calculated both from the gradient of the fluid temperature in the vicinity of the heated plate, and from the electrical input to the heater. Both values were in good agreement for water, but the latter was 30–40% larger than the former for air because radiation loss from the heater to the environment took a relatively large portion of the total heat flux. The former method was, therefore, adopted to obtain the heat flux in the present experiment. Thermal properties in the non-dimensional numbers of Ra^* and Nux were estimated at the reference temperatures T_f as $T_f = (3T_w + T_\infty)/4$ for air and as $T_f = (T_w + T_\infty)/2$ for water, respectively, which have been employed by the previous workers.

As is obvious from the Fig. 2, the local Nusselt numbers in a laminar region coincide with the analytical solutions of Fujii *et al.* [9]. Also in a turbulent region, the data agree well with those of the previous experiments by Miyamoto *et al.* [10] for air and Vliet and Liu [2] for water, respectively. Furthermore, their results can be extrapolated to the high Ra^* number region. The present results indicate that the laminar and turbulent regions can be classified by using the Rayleigh numbers, i.e. laminar region; $Ra^* < 3 \times 10^{11}$ and $Ra^* < 5 \times 10^{12}$, and turbulent region; $Ra^* > 10^{12}$ and $Ra^* > 1.5 \times 10^{13}$ for air and water, respectively. The data for the apparatus No. I and II give almost the same results with those for the No. III.

3.2. *Streaky patterns on the heat transfer surface*

The surface temperature distributions of the heated plate were visualized by using the liquid crystal sheet. The illustrative sets of visualized photos are presented in Fig. 3. The photos (a), (b), (c) and (d) correspond to the laminar, transition, relatively low Ra^* turbulent, and high Ra^* turbulent regimes, respectively.

In the laminar region, the color is almost the same throughout the sheet and represents the uniform

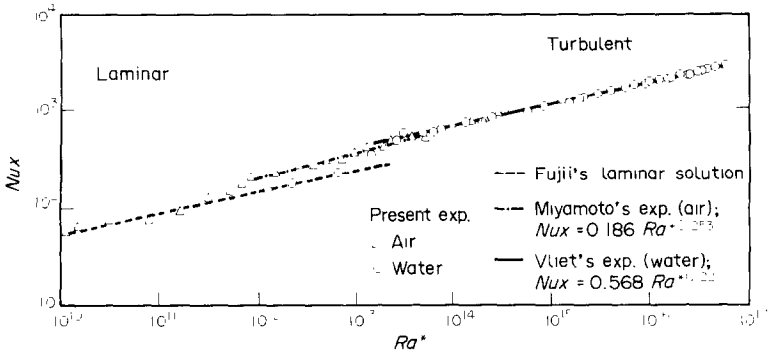

FIG. 2. Local Nusselt numbers in a turbulent region of natural convection along a vertical flat plate heated with uniform heat flux.

temperature distribution. Near the onset of transition, horseshoe-shaped low temperature regions are observed as shown in Fig. 3(b). They are generated intermittently at an equal time interval and at a fixed location of the heated surface. The time interval between these generations is about 4 s in the present experiments. This value agrees well with the frequency of most amplified disturbances predicted from a stability analysis by Qureshi and Gebhart [11], and also with the formation interval of a vortex street generated in the transition region of a natural convection boundary layer, which was observed by Fujii [12] experimentally. These result suggest that the patterns of the surface temperatures well reflect the actual phenomena occurring in the boundary layer.

With the increase of Ra^*, it is revealed that the horseshoe patterns on the surface break into streaky patterns elongated in the flow direction as is shown in Fig. 3(c). These streaky patterns are also found in the higher Ra^* region as presented in Fig. 3(d). As is obvious from the figures, the sizes of these streaky patterns are very large and distributed randomly. The streaky patterns of the heated surface exhibit the non-uniform temperature distributions not only in the flow direction but also in the spanwise direction normal to the flow even in the case that the thermal boundary condition is considered two-dimensional as for the present experiment.

The visualized surface temperatures on a constant heat flux wall also illustrate the instantaneous distributions of the local heat transfer coefficients. In other words, the heat transfer coefficients in the turbulent region can be closely correlated with the generation, passage, and disappearance of these large scale patterns. Therefore, it is very important to obtain the qualitative and quantiative information about these patterns.

3.3. *Structure of the turbulent boundary layer of natural convection*

The streaky patterns mentioned in the previous section are considered as the consequence of large eddy motions that exist in the turbulent boundary layer. Therefore, the flow visualizations within the turbulent boundary layer of water were conducted to investigate the structures of large eddies.

Figures 4(a) and (b) represent the visualized flow field near the heated wall by using a hydrogen-bubble method, where the cathode wire is stretched horizontally at the locations of $\zeta = 0.86\,(Y^+ \simeq 10)$ and $\zeta = 4.9\ (Y^+ \simeq 57)$ from the wall, respectively. The photos were taken from the lower right-hand side facing the front of the heated surface in order to visualize the flow field stereoscopically. As is apparent from both figures, the time-lines of bubbles show the non-uniform velocity distributions in the spanwise direction and also the streaky patterns appear in the flow direction. The portions of high velocity are ejected from the wall and the low velocity regions flow toward the wall. It is also obvious from the photos that the vortex motions with the longitudinal axes are dominant in the boundary layer. Almost the same phenomena are observed in the entire regions of the boundary layer except for the nearest location to the wall, where the bubbles attached on the surface render the flow invisible.

Although it is rather qualitative to deduce the following results from these photos, the visualized fluid motions of high-speed ($u' > 0$) ejections ($v' > 0$) and low-speed ($u' < 0$) inflows ($v' < 0$) both give the negative values of Reynolds shear stress ($-u'v'$). The quantitative data of Reynolds shear stress distributions measured by the previous workers are illustrated in Fig. 5 together with the relevant experimental conditions tabulated in Table 2. The abscissa in Fig. 5 is the normalized distance ζ from the wall, and the locations of the present visualizations are shown with the arrays. Hishida *et al.* [5] obtained the result $-\overline{u'v'} > 0$ in the region of $\zeta < 10$, and their data conflict with our visualizations, which well explain the results of Miyamoto *et al.* [6] and Smith [3] except in the very near wall region.

The combined visualizations by the liquid crystal sheet patched on the heated surface and the hydrogen bubbles generated at the several locations from the wall were conducted to ascertain the correlations between streaky patterns and fluid motions in the boundary

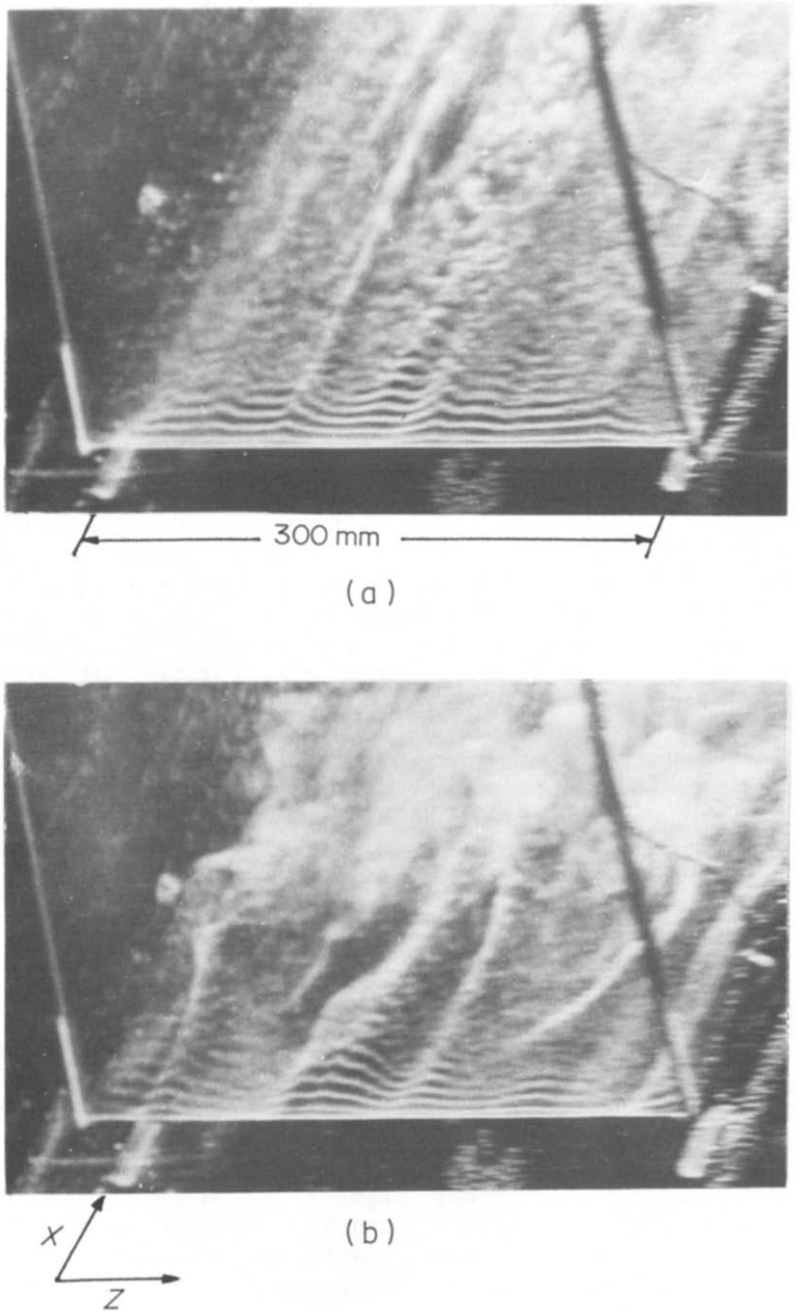

FIG. 4. Visualization of the structure of turbulent natural convection boundary layer by using a hydrogen-bubble method. $Ra^* = 2.7 \times 10^{14}$, wire location, (a) $\zeta = 0.86 (Y^+ \simeq 10)$ and (b) $\zeta = 4.9$ $(Y^+ \simeq 57)$.

Table 2. Experimental conditions of the previous works presented in Fig. 5

Reference	Method	Fluid	Heated plate	Ra^*
Smith [3]	CTA	air	isothermal	1.42×10^{13}†
Hishida *et al.* [5]	CTA	air	isothermal	5.14×10^{13}†
Miyamoto *et al.* [6]	LDV	air	constant heat flux	1.06×10^{14}

† Ra for isothermal plate is transformed into modified Ra^* by using the relation; $Ra^* = Ra \cdot Nu_x$.

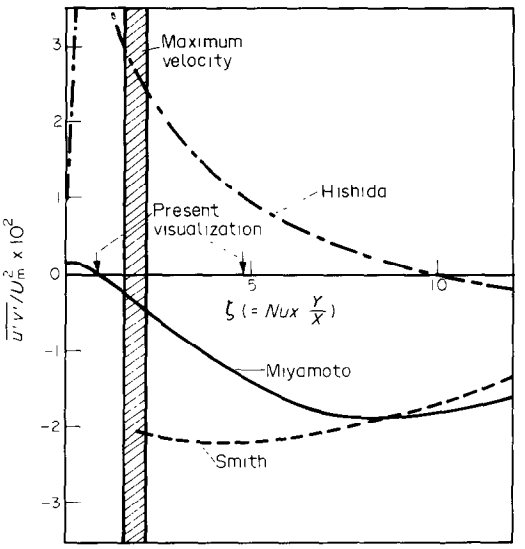

FIG. 5. Reynolds shear stress distributions in the wall region obtained by the previous workers.

layer. The representative photos are presented in Fig. 6(a), (b) and (c).

In the near wall region as presented in Fig. 6(a) and (b), the time-lines of hydrogen-bubbles are, in many cases, elongated to the vertical direction in the high temperature regions of the surface and recessed in the low temperature regions. The above results suggest that the streaky patterns on the heated surface are caused by the fluid motions, which consist of the low temperature ($t' < 0$) and low velocity ($u' < 0$) inflow ($v' < 0$) toward the wall, and of the high temperature ($t' > 0$) and high velocity ($u' > 0$) ejection ($v' > 0$) from the wall. The above information is rather qualitative but yields the positive values of velocity and temperature correlations, i.e. $u't' > 0$ and $v't' > 0$, which agree with the data of refs [5] and [3]. Also from Fig. 6(c), the portion of high temperature and high velocity are observed to be ejected toward the outer region of the boundary layer.

In order to investigate the structure of turbulent boundary layer in more detail, the flow visualizations in the X–Y plane were performed and the typical set of photos for the inflow and ejection stages of the fluid motions are presented in Figs. 7(a) and (b), respectively. The cathode wire was stretched normal to the wall. The photos were taken at a constant time interval. The surface temperature and the fluid temperature at the location of $\zeta = 1$ are monitored and confirmed to be low and high in each case of inflow and ejection. In the inflow stage, the velocities near the wall are apparently smaller than those in the ejection stage, while the bubbles are generated at the same and constant time intervals in both cases. The former flow is directed to the wall in contrast to the outward flow in the ejection stage.

It is found that the velocity and temperature fields within the boundary layer are altered significantly through the course of eddy motions mentioned above. These observations have led us to the conjecture that the large eddy motions play an important role in determining the structures of turbulent boundary layer.

3.4. *Time and length scale of large eddies*

The quantitative information about the large eddies is not only indispensable for investigating the structures of turbulent boundary layer, but will also give the explanatory models for the turbulent transport. Thus, in the present section, the scales of these large eddies are measured for both cases of water and air. In examining these, time and length scales should be clearly distinguished. Besides, the locations for measuring these scales must be described together with the detection schemes.

Water. In the present experiment of water, the length scales λ of the large eddies are represented as the spanwise (horizontal) distances between the adjacent pair of streaks in the surface temperature distributions as were presented in Figs. 3(c) and (d). The time scales f are also defined as the frequencies of streaks, which pass through a fixed point of heated surface per unit time. These length and time scales are deduced from those for the bursting phenomena in forced convection and can be easily measured from the recorded data of surface temperature distributions on the liquid crystal sheet. Another measuring technique is also utilized to obtain these scales, by means of the short time correlations of temperature fluctuations in the wall region. This method is based on similar ideas as for the bursting phenomena in a forced convection. Personal errors, which are inevitable in visualization studies, will be excluded by this method.

The temperature fluctuations are measured at a fixed location of $\zeta = 1.2(Y^+ \simeq 14)$ from the wall by a single probe and their signals are calculated to yield the coefficients of the short time auto-correlations R_τ with the time-delay τ. Also, the signals from a pair of probes, one is fixed and another is traversed in the spanwise direction, are computed to obtain the short time cross-correlation coefficients R_z with the distance Z between two probes.

Thus obtained results with the auto- and cross-correlation coefficients are illustrated in Figs. 8(a) and (b), respectively. Under the adequate conditions of sampling frequencies and data volumes mentioned in section 2.3, the correlation coefficients R_τ and R_z both decrease monotonously from a unity at $\tau = 0$ and $Z = 0$ with the increase of τ and Z, respectively, and then show the second peaks at certain values of τ and Z, respectively. These time-delay τ and spanwise distance Z corresponding to the second maximums of coefficients can be defined as the time interval, which is the inverse of frequency f, and the spanwise distance λ between the streaks averaged for a short time, respectively. The frequencies f and the spanwise distance λ obtained by the visualization are both scattered owing to the randomness of a turbulence.

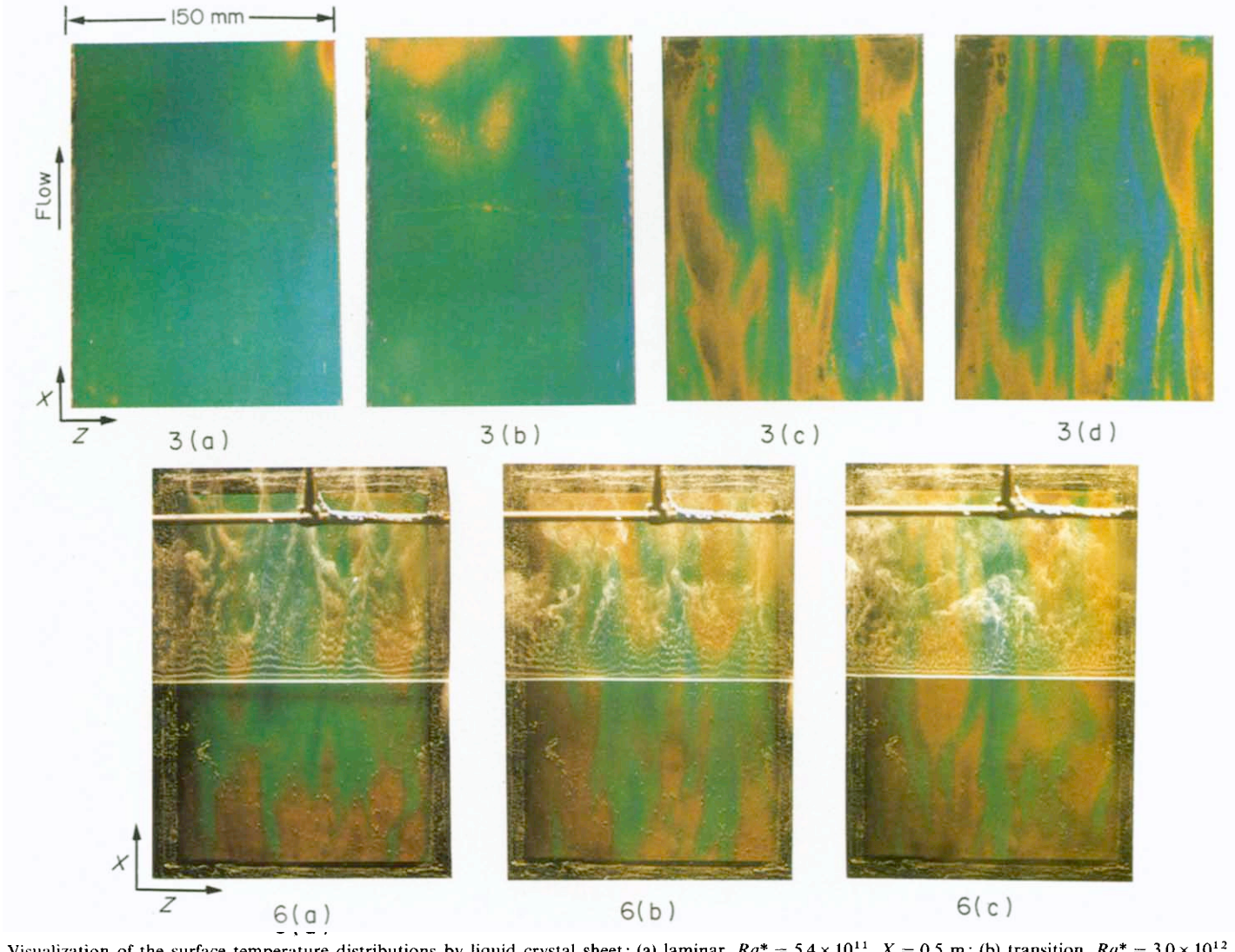

FIG. 3. Visualization of the surface temperature distributions by liquid crystal sheet: (a) laminar, $Ra^* = 5.4 \times 10^{11}$, $X = 0.5$ m; (b) transition, $Ra^* = 3.0 \times 10^{12}$, $X = 0.5$ m; (c) turbulent, $Ra^* = 2.7 \times 10^{14}$, $X = 2.1$ m; and (d) turbulent, $Ra^* = 5.4 \times 10^{16}$, $X = 5.5$ m.

FIG. 6. Combined visualizations of surface temperature distribution and flow field in the wall region. $Ra^* = 2.7 \times 10^{14}$, $X = 2.1$ m, wire location, (a) $\zeta = 0.86 (Y^+ \simeq 10)$; (b) $\zeta = 2.6 (Y^+ \simeq 30)$; and (c) $\zeta = 8.6 (Y^+ \simeq 100)$.

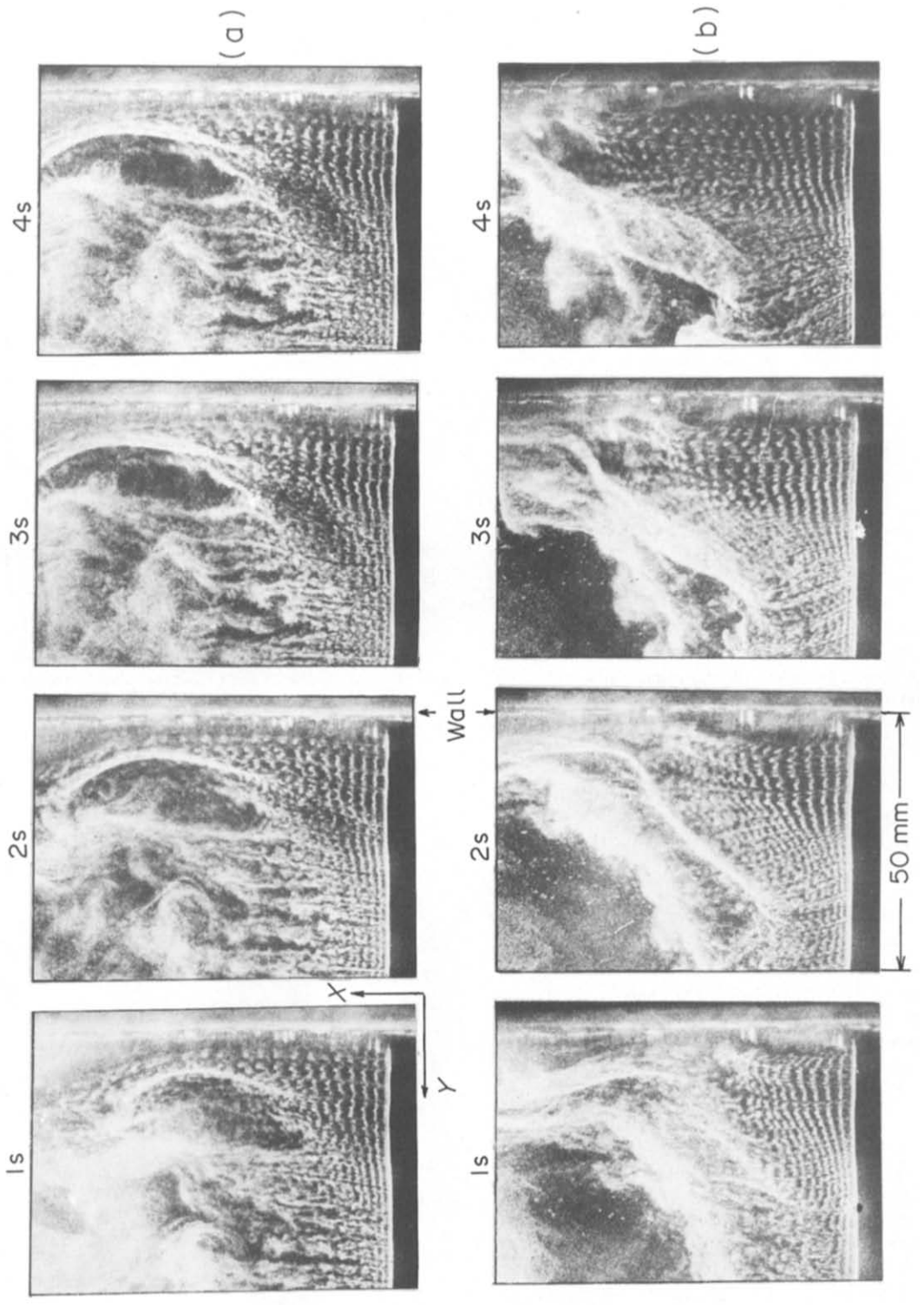

FIG. 7. Inflow and ejection stages of large eddy motion. $Ra^* = 2.7 \times 10^{14}$, $X = 2.1$ m, (a) inflow and (b) ejection.

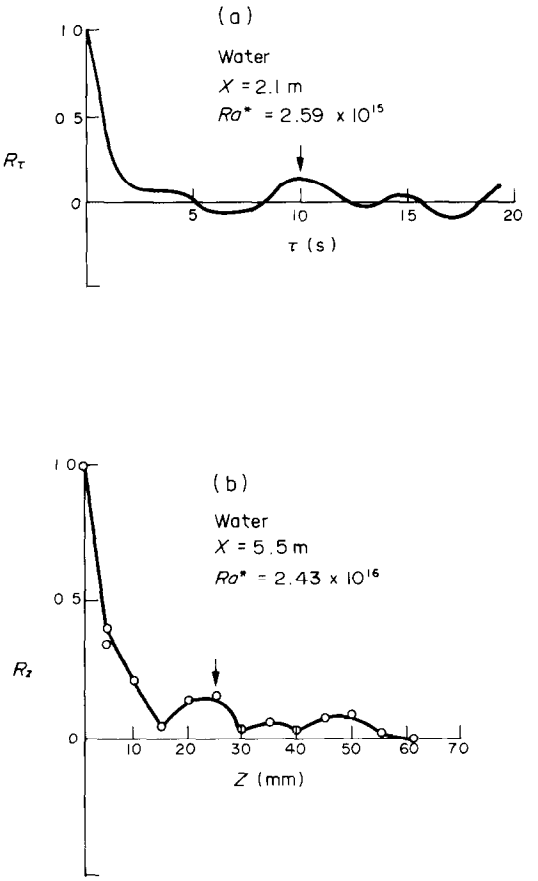

FIG. 8. Typical examples of short-time auto- and cross-correlation curves: (a) auto-correlation and (b) cross-correlation.

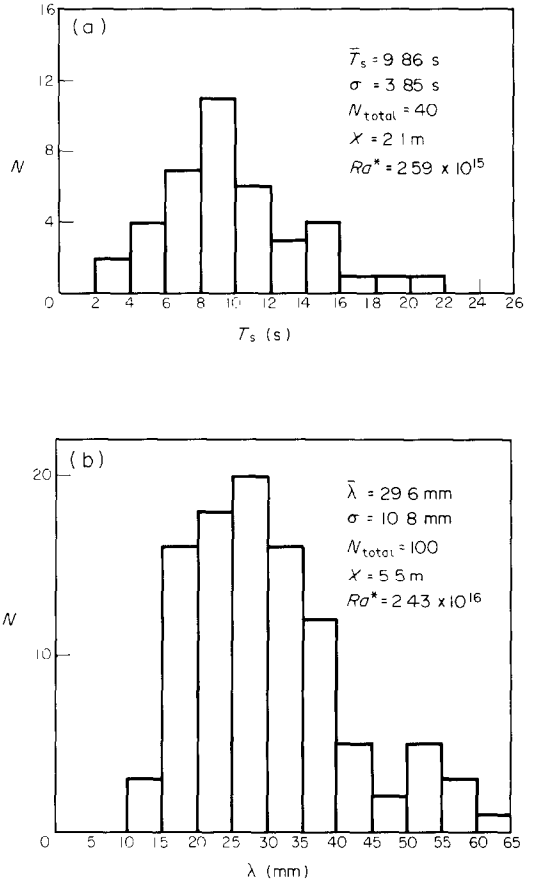

FIG. 9. Histograms of time interval between streaks and streak spacing: (a) time interval and (b) streak spacing.

Figures 9(a) and (b) show the representative histograms of the time between streaks $T_s (= 1/f)$ and of the streak spacing λ from the visual data, respectively. The standard deviations about the mean values are very large as shown in both figures. Nevertheless, the averaged data with a number of experiments under the same conditions can provide the available results.

The averaged data of streak spacings λ and the frequencies of streaks f are presented in Figs. 10 and 11, respectively, with the surface heat flux q_w as an abscissa. As is obvious from both figures, the data obtained from the visualization coincide fairly well with those from the correlation coefficients. The values of λ decreases from 40 to 25 mm and f increases from 3 to 10 cycles min^{-1} with the increase of heat flux. These results indicate that the spanwise lengths and frequencies of large eddies are strongly affected by the surface heat flux, and are insensitive to the height X from the bottom of the test plate. The latter result can also be considered as one of the corroborations that the local heat transfer coefficients are almost independent from the height and become nearly constant throughout the turbulent regime under the fixed value of surface heat flux.

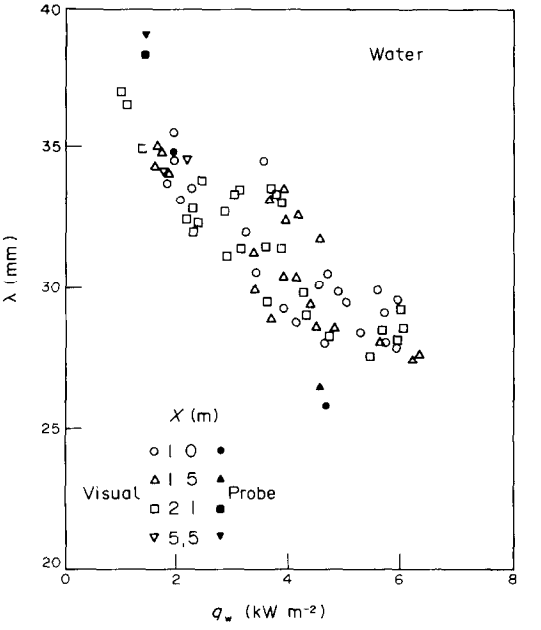

FIG. 10. Averaged streak spacings for water.

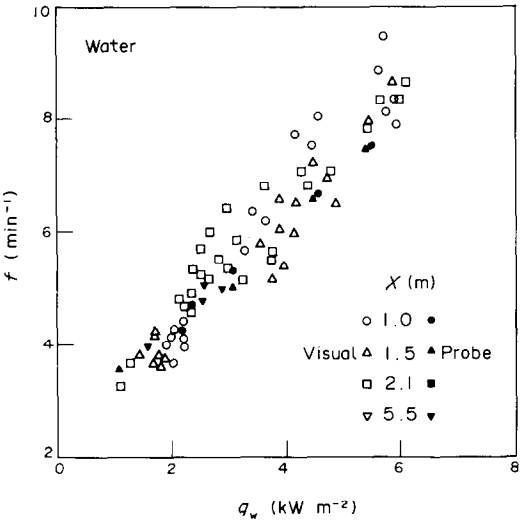

FIG. 11. Averaged frequencies of streaks for water.

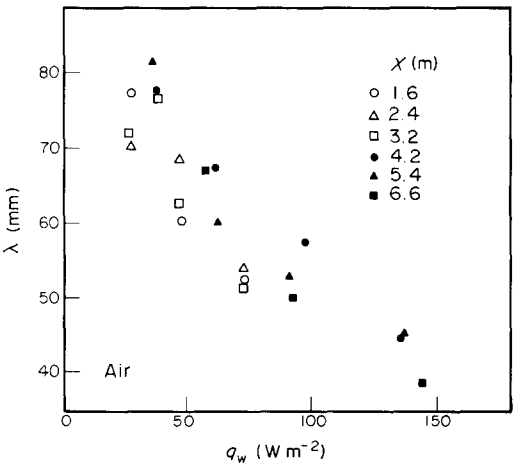

FIG. 13. Averaged streak spacings for air.

Air. It is most advantageous to determine the scales of large eddies from the visualized data of liquid crystal sheet because both scales can be measured simultaneously. As for the present case of air, several trials have been made to visualize the temperature distributions on the heated surface but failed. This is mainly due to the thermal capacity of air, which is much smaller than that of liquid crystal sheet. Therefore, another measuring technique is adopted in this experiment.

The visualization of flow fields in the wall region are performed by using a smoke-wire method to obtain the spanwise distance λ for air. The smoke-wire method utilized in this experiment is as follows: a fine nichrome wire, on which liquid paraffin was painted, was placed at the fixed position $\zeta = 1.2(Y^+ \simeq 25)$ from the wall and impulsively heated by DC current. After a certain time delay from a smoke generation, a stroboscope was flashed to take the photos.

Typical examples of thus visualized data are presented in Figs. 12(a) and (b). Both figures (a) and (b), which were taken simultaneously, represent the instantaneous velocity distributions in the X–Z and Y–Z planes, respectively. In many cases in these photos, the fluid portions of the low streamwise velocity flow towards the wall and the high velocity regions are ejected from the wall. The former regions refer to the low temperature regions of the heat transfer surface based on the previous discussions in section 3.3. Therefore, the spanwise distances between these portions are regarded as the same as those defined for water. The spanwise lengths of air are measured with a large number of the photos and averaged with each experimental condition. On the other, the frequencies of streaks are obtained from the auto-correlation coefficients of temperature fluctuations in the near wall region. This method follows the procedure in case of water.

The spanwise distances and the frequencies of streaks for air are plotted with the surface heat flux and represented in Figs. 13 and 14, respectively. Both figures show that the values of λ decrease from 80 to 40 mm, and

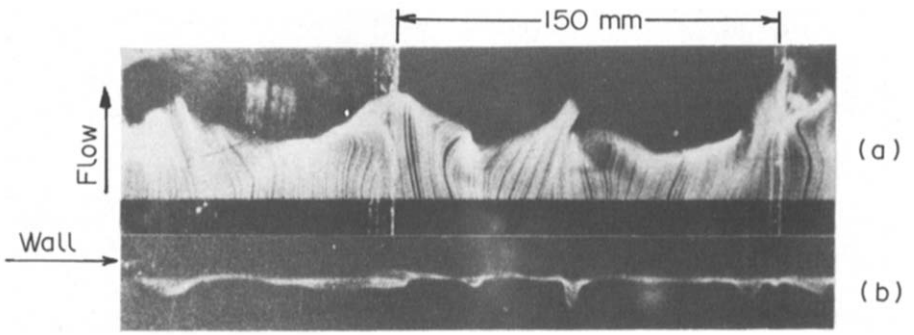

FIG. 12. Visualization of instantaneous velocity distribution in the wall region of turbulent natural convection boundary layer by a smoke-wire method. $Ra^* = 5.2 \times 10^{13}$, $X = 3.2$ m, wire location $\zeta = 1.2$ ($Y^+ \simeq 25$), (a) X–Z plane and (b) Y–Z plane.

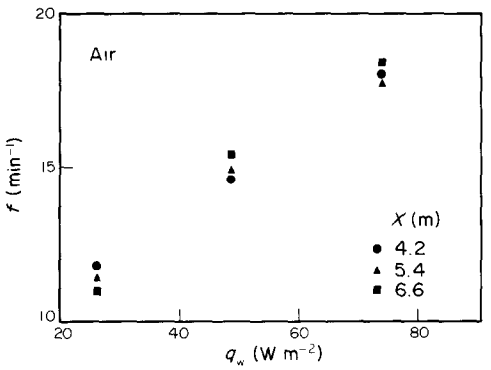

FIG. 14. Averaged frequencies of streaks for air.

f increases from 12 to 18 cycles min^{-1} with the increase of heat flux, in the range of our experiments. It is also revealed that the spacings λ and frequencies f of streaks are free from the height X from the bottom of the test plate. This result is almost the same as that obtained for water.

3.5. *Coherency of large eddies*

It is very important to investigate whether the coherent or ordered structures, which have been already found with the bursting phenomena in a forced convection, also exist in the turbulent natural convection boundary layer. Therefore, in the present section, the spanwise length λ and frequencies f of the large eddies are rearranged and normalized by the characteristic length and time scales in order to ascertain that the non-dimensional scales can provide constant values independent from properties of fluid, Ra^* numbers, and sizes of heated plate. The studies were conducted with various characteristic length and time scales by trial and error. The same normalization scheme as for the bursting phenomena is tested using the characteristic length scale ν/u^*, where u^* is the friction velocity, but the normalized data are scattered in both cases of air and water. The physical meanings of the above characteristic length scale are not so well-grounded in a natural convection as in a forced convection.

Among these trials of the normalization, the data are best rearranged by adopting the characteristic length scale λ_L; $\lambda_L = (\kappa\nu^2/g\beta q)_w^{1/4}$ and the characteristic time scale f_T; $f_T = (\nu/\lambda_L^2)_w$, respectively. The measured spanwise spacings λ and frequencies f obtained from both cases of air and water with different sizes of heat transfer plate are normalized by using the above characteristic scales λ_L and f_T.

The results are plotted with Ra^* and shown in Figs. 15 and 16, respectively. It is shown from Fig. 15 that the normalized values $\hat{\lambda}$ $(= \lambda/\lambda_L)$ become constant at around 50 in the wide range of Ra^* from 10^{12} to 10^{17} and are the comparable order of magnitude to the boundary-layer thickness. The normalized length scale $\hat{\lambda}$ can be also considered as the modified Grashof number $Gr_\lambda^*(= g\beta q_w/\kappa\nu^2 = \hat{\lambda}^4)$ of which characteristic length is λ. This result indicates that the Grashof numbers based on the streak spacings λ become nearly constant throughout the turbulent region and is very interesting when compared with the bursting phenomena, where the Reynolds numbers $Re(= u^*\lambda/\nu)$ based on the streak spacings λ become almost constant.

Furthermore, the normalized frequencies $\hat{f} = f/f_T$ are consistent at approximately 0.03 in the range of Ra^* from 10^{13} to 10^{17} as is obvious from Fig. 16. The characteristic time scale $f_T = \nu/\lambda_L^2$ employed here can be simply rewritten as $f_T = (g\beta q/\kappa)_w^{1/2}$, and this suggests that the non-dimensional frequencies of streaks are apparently independent from viscosity and thermal diffusivity of the fluid.

The above discussions conducted with the heated wall of a constant heat flux, are considered applicable to the case of an isothermal wall. It has been well known that the heat transfer characteristics in the turbulent region of a natural convection were unaffected by the thermal boundary conditions of the heated plate and were transformable with each other. Actually, our test plate gave almost the constant temperature distributions in a turbulent regime by averaging for a long period.

From these facts, the following characteristic time and length scales for the constant heat flux

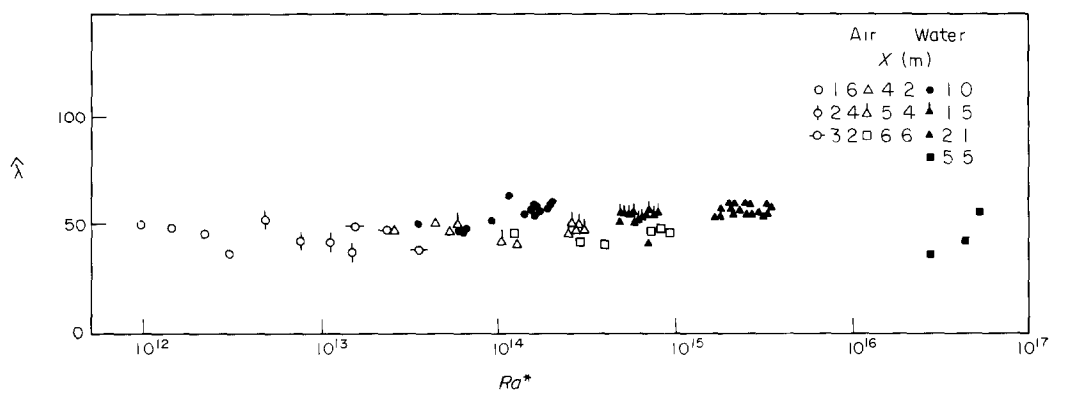

FIG. 15. Non-dimensionalized streak spacings.

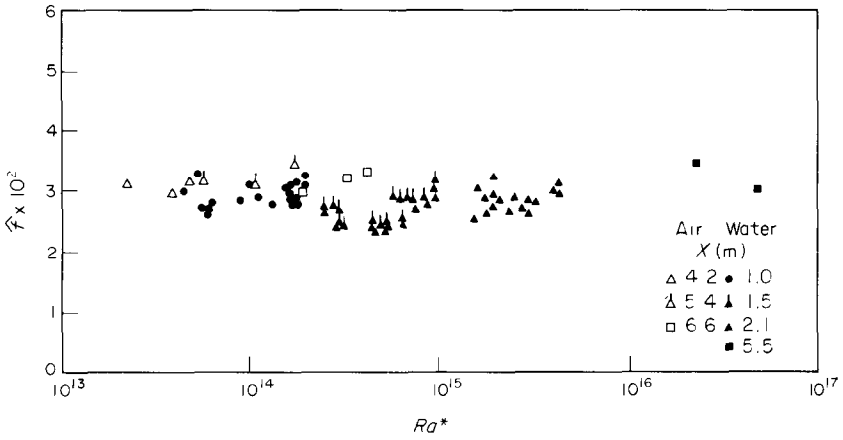

FIG. 16. Non-dimensionalized frequencies of streaks.

wall are transformed in order to apply them for the isothermal plate; these are the length scale $\lambda_L' = [\nu^2/g\beta(T_w - T_\infty)]^{1/3}$ and the time scale $f_T' = \nu/\lambda_L^2$ instead of λ_L and f_T, respectively. By using these characteristic scales, the present data are normalized and provide the results that the normalized spanwise spacings $\hat{\lambda}'$ and frequencies of streaks $\hat{f}'$ become constants at around 80 and 0.01, respectively.

These results suggest that the coherent or ordered structures exist in the large eddy motions. Moreover, the series of the visualized data obtained in the present study indicate that the buoyancy-induced turbulent boundary layer is more violent than has been imagined. The velocity and temperature profiles within the turbulent boundary layer are determined from the consequence of generation, passage, and disappearance of the large eddies, of which sizes are comparable to the boundary-layer thickness.

4. CONCLUDING REMARKS

The present study has been conducted to investigate experimentally the transport mechanisms of heat and momentum in a turbulent boundary layer of natural convection along a vertical flat plate. Special attentions were paid to the large eddy motions which exist in the turbulent boundary layers of both air and water.

The surface temperature distributions of the constant heat flux wall were visualized by using the liquid crystal sheet, and the streaky patterns of large scales in space and time were found in a turbulent regime. These streaky patterns were caused by the large eddy motions existing in the turbulent boundary layer and exert the serious influences on the turbulent heat transfer.

The large eddy motions were observed by using the combined visualization techniques of hydrogen bubbles and liquid crystal sheet, and it was revealed that a series of eddy motions consist of low-temperature and low-velocity inflow from the outer region of the boundary layer and high-temperature and high-velocity ejection from the wall.

The measurements with the length and time scales of these large eddies in the wall region were performed for both water and air in order to obtain the quantitative information about the turbulent transport. It was found that the time and length scales were strongly affected by the surface heat flux of the heated plate, and insensitive to the height from the bottom of the test plate.

The coherent or ordered structures of these large eddies in the wall region were also investigated by normalizing the above data with the characteristic length and time scales. The values of these normalized length and time scales for both air and water and with the different sizes of the test plates were revealed to become almost constant over a wide range of Ra^*. The above results suggest that the coherent or well-ordered structures in large eddy motions are dominant in the turbulent boundary layer, and play an important role on the turbulent transport of heat and momentum.

Acknowledgement—Authors wish to acknowledge the financial support from the Ministry of Education, Science, and Culture of Japan through a research grant (No. 5875041).

REFERENCES

1. R. Cheesewright, Turbulent natural convection from a vertical plane surface, *Trans. Am. Soc. mech. Engrs.*, Series C, *J. Heat Transfer* **90**, 1–8 (1968).
2. G. C. Vliet and C. K. Liu, An experimental study of turbulent natural convection boundary layer, *Trans. Am. Soc. mech. Engrs.*, Series C, *J. Heat Transfer* **91**, 517–531 (1969).
3. R. R. Smith, Characteristics of turbulence in free convection flow past a vertical plate, Ph.D. thesis, University of London (1972).
4. C. J. Hoogendoorn and H. Euser, Velocity profiles in the turbulent free convection boundary layer, *Proc. 6th Int. Heat Transfer Conf.*, vol. 2, pp. 193–198 (1978).
5. M. Hishida, Y. Nagano, T. Tsuji and I. Kaneko, Turbulent boundary layer of natural convection along a vertical flat

plate, *Trans. Japan Soc. mech. Engrs* **47,** 1260–1268 (1981) in Japanese.
6. M. Miyamoto, H. Kajino, J. Kurima and I. Takanami, Development of turbulence characteristics in a vertical free convection boundary layer, *Proc. 7th Int. Heat Transfer Conf.*, vol. 2, pp. 323–328 (1982).
7. S. J. Kline, W. C. Reynolds, F. A. Schraub and P. W. Runstadler, The structure of turbulent boundary layer, *J. Fluid Mech.* **30,** 741–773 (1967).
8. N. Kasagi, Liquid crystal application in heat transfer experiments, IL-27, Thermoscience Div., Mech. Engr. Dept., Stanford University, Stanford, California (1980).
9. T. Fujii, M. Takeuchi, M. Fujii, K. Suzaki and H. Uehara, Experiments on natural-convection heat transfer from the outer surface of a vertical cylinder to liquids, *Int. J. Heat Mass Transfer* **13,** 753–783 (1970).
10. M. Miyamoto, H. Kajino, J. Kurima and I. Takanami, Development of turbulence characteristics in a vertical free convection boundary layer, *Proc. 18th National Heat Transfer Symposium*, Japan, pp. 295–297 (1981) in Japanese.
11. Z. H. Qureshi and B. Gebhart, Transition and transport in a buoyancy driven flow in water adjacent to a vertical uniform flux surface, *Int. J. Heat Mass Transfer* **21,** 1467–1479 (1978).
12. T. Fujii, On the generation of a vortex street in the free-convection boundary layer, *Trans. Japan Soc. mech. Engrs* **24,** 973–977 (1958) in Japanese.

STRUCTURE A GRANDS TOURBILLONS ET TRANSFERT THERMIQUE DE CONVECTION NATURELLE LE LONG D'UNE PLAQUE PLANE VERTICALE

Résumé—On étudie expérimentalement le transfert turbulent en convection naturelle. L'attention est portée sur les mouvements à grand tourbillon qui existe dans une couche limite turbulente le long d'une plaque plane verticale. Des visualisations des champs de température et de vitesse dans la région pariétale sont faites et elles révèlent que les mouvements à large tourbillon jouent un rôle important sur le transfert turbulent. Les échelles de longueur et de temps de ces tourbillons sont définis et mesurés. On discute aussi la structure cohérente des tourbillons.

WIRBELSTRUKTUR UND WÄRMEÜBERGANG BEI DER TURBULENTEN NATÜRLICHEN KONVEKTION LÄNGS EINER VERTIKALEN EBENEN PLATTE

Zusammenfassung—Der turbulente Transport bei natürlicher Konvektion wurde experimentell untersucht. Das Hauptinteresse galt der Bewegung großer Wirbel innerhalb der turbulenten Grenzschicht entlang einer vertikalen ebenen Platte. Ziel der Untersuchung war das Sichtbarmachen der Temperatur- und Geschwindigkeitsfelder in der Wandzone, und es stellte sich heraus, daß die Bewegung großer Wirbel eine wichtige Rolle beim turbulenten Wärmetransport spielt. Die Größenordnung der Wirbel (Länge und Zeit) wurde definiert und gemessen. Ferner wurde die kohärente Struktur der Wirbel diskutiert.

КРУПНОВИХРЕВАЯ СТРУКТУРА И ЕСТЕСТВЕННОКОНВЕКТИВНЫЙ ТУРБУЛЕНТНЫЙ ТЕПЛОПЕРЕНОС ВДОЛЬ ПЛОСКОЙ ВЕРТИКАЛЬНОЙ ПЛАСТИНЫ

Аннотация—Исследовался турбулентный теплоперенос в естественной конвекции. Особое внимание уделено крупным вихревым структурам, существующим в турбулентном пограничном слое вдоль плоской вертикальной пластины. В основном проводилась визуализация полей температуры и скорости в пристенной области. Найдено, что крупновихревые движения играют важную роль при турбулентном переносе. Определены и измерены масштабы длин и времени этих вихрей. Также обсуждалась когерентная структура вихрей.